Angular dependence of circular dichroism in Pb-doped and pristine $Bi_2Sr_2CaCu_2O_{8+\delta}$

V. Arpiainen,[1] V. Zalobotnyy,[2] A. A. Kordyuk,[2,3] S. V. Borisenko,[2] and M. Lindroos[1]
[1]*Institute of Physics, Tampere University of Technology, P.O. Box 692, FIN-33101 Tampere, Finland*
[2]*Leibniz-Institute for Solid State Research, IFW-Dresden, P.O. Box 270116, D-01171 Dresden, Germany*
[3]*Institute of Metal Physics, National Academy of Sciences of Ukraine, 03142 Kyiv, Ukraine*
(Received 9 October 2007; published 24 January 2008)

We have investigated both experimentally and computationally angle-resolved photoemission spectroscopy spectra of $Bi_2Sr_2CaCu_2O_{8+\delta}$ and $(BiPb)_2Sr_2CaCu_2O_{8+\delta}$ with circularly polarized light. The large circular dichroism in the angular distribution of photoelectrons is reproduced by nonmagnetic one-step calculations within dipole approximation. A strong dependence of spectral weight on experimental parameters, especially on excitation energy, is found.

DOI: 10.1103/PhysRevB.77.024520 PACS number(s): 74.72.−h, 79.60.−i, 71.18.+y, 74.72.Hs

I. INTRODUCTION

In recent years, the angle-resolved photoemission spectroscopy (ARPES) studies of high-T_c superconductors with circularly polarized light have attracted wide interest. A great deal of this has been due to the possible verification of the time-reversal symmetry breaking.[1,2] Experiments have been made, but the results are controversial.[3–5] In the studies of Bi2212, it was found that, within a certain experimental setup, the bilayer split bands have different signs of the circular dichroism signal $I_r - I_l$, that is, the difference between intensities of photoelectron excitation when changing light helicity from right-handedly (RH) to left-handedly polarized light (LH).[6] The explanation for the different signs was not found, but the discovery was successfully used in studies of bilayer splitting[6] and parity of the pairing bosons[7] in Bi2212.

Circular dichroism in the angular distribution (CDAD) from nonchiral, oriented molecules was first predicted by Ritchie.[8] Later, it was shown that CDAD occurs in the electric dipole transition,[9] and is therefore by orders of magnitude stronger than dichroism from chiral molecules due to the interference of electric and magnetic dipole transitions.[10] For oriented linear molecules, criterion for the appearance of CDAD is that experimental setup exhibits a definite handedness, where the direction of incoming photon **q**, molecular axis **n**, and photoelectron momentum **k** are noncoplanar. In nonlinear oriented molecules and solids, CDAD vanishes because of symmetry selection rules only if both **q** and **k** lie on a symmetry plane of the sample.[11,12]

The origin of the CDAD within the dipole transition is in the matrix element effects,[10,13,14] and besides the selection rules arising from crystal symmetry, the CDAD can be accurately studied only through photoemission simulations. In this paper, we compare one-step simulations of ARPES with circularly polarized light to experimental results. Similar calculations have been successfully performed for Al(111) (Ref. 15) and Ni(111),[16] but not for a complex layered structure. We focus on Fermi surface maps and CDAD patterns with two photon energies. In addition to qualitative comparison, we compare normalized dishroism signals. We find that calculations are in close agreement with experiments, and that CDAD is to a high degree excitation energy dependent.

II. THEORY

In the one-step model,[17,18] the ARPES intensity can be expressed as

$$I(\mathbf{k}_\parallel, \epsilon_f) = -\frac{1}{\pi}\Im\langle \mathbf{k}_\parallel, \epsilon_f | G_2^+ \Delta G_1^+ \Delta^\dagger G_2^- | \mathbf{k}_\parallel, \epsilon_f \rangle, \tag{1}$$

where $|\mathbf{k}_\parallel, \epsilon_f\rangle$ is a free-electron state with energy ϵ_f and parallel momentum $\mathbf{k}_\parallel$ that is determined by ϵ_f and the position of the detector. $G_2^\pm$ is the retarded (+) or advanced (−) Green's function for the electron at high energy, and G_1^+ is the Green's function for the photohole. $G_2^-|\mathbf{k}_\parallel, \epsilon_f\rangle = |f\rangle$ is a time-reversed low-energy electron diffraction (LEED) state. Green's functions are quasiparticle propagators, and the finite lifetime of quasiparticles is taken into account in the imaginary part Σ'' of Green's function's self-energy. The imaginary part of the self-energy Σ_i'' of the hole propagator gives a finite linewidth to the initial state and spreads the intensity features. Σ_f'' of the high-energy electron spreads the final state and intensity features as a function of excitation energy, but it also determines the penetration depth of the LEED-type final state electrons.[19] Using spectral function representation,

$$-\frac{1}{\pi}\Im G_1^+ = \sum_i B_{ii} |i\rangle\langle i|, \tag{2}$$

where the Green's function for the photohole is written as a sum of spectral functions B_{ii} over initial states, ARPES intensity can be expressed as

$$I(\mathbf{k}_\parallel, \epsilon_f) = \sum_i B_{ii} |\langle f|\Delta|i\rangle|^2. \tag{3}$$

Within the Coulomb gauge, keeping only the lowest order terms of the vector potential **A**, the interaction Hamiltonian in atomic units is given by

$$\Delta = \frac{\mathbf{A}\cdot\mathbf{p}}{c} = \frac{\mathbf{A}\cdot\nabla V}{\omega c}, \tag{4}$$

where **p** is the momentum operator, ω is the energy of the photon in atomic units where $\hbar = 1$, and V is the crystal potential. In the expression

 ©2008 The American Physical Society

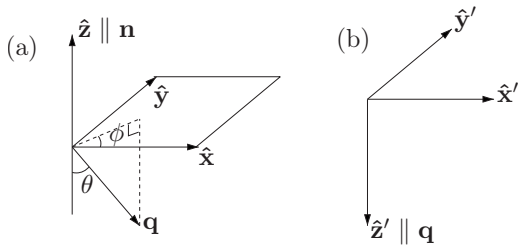

FIG. 1. (a) Right-handed coordinate system of the sample. (b) Left-handed coordinate system of the incoming photon. Within the normal incidence setup, where $\theta=0$ and $\phi=0$, $\hat{\mathbf{x}}'=\hat{\mathbf{x}}$, $\hat{\mathbf{y}}'=\hat{\mathbf{y}}$, and $\hat{\mathbf{z}}'=-\hat{\mathbf{z}}$.

$$\mathbf{A} = \frac{\mathbf{a}}{2} e^{i\mathbf{q}\cdot\mathbf{r}} = a\frac{\hat{\mathbf{e}}}{2} e^{i\mathbf{q}\cdot\mathbf{r}} \tag{5}$$

for the vector potential, a is normalized to unit photon per unit time and $\hat{\mathbf{e}}$ is the polarization vector. For circularly polarized light, the polarization vector is a complex combination $\frac{\mathbf{x}'-i\mathbf{y}'}{\sqrt{2}}$ for left-handed polarization and $\frac{\mathbf{x}'+i\mathbf{y}'}{\sqrt{2}}$ for right-handed polarization. $\hat{\mathbf{x}}'$ and $\hat{\mathbf{y}}'$ are unit vectors in the left-handed Cartesian coordinate system of the incoming photon in Fig. 1(b), where $\hat{\mathbf{z}}' \| \mathbf{q}$ and $\hat{\mathbf{y}}'$ is always parallel to sample surface. Substitution to Eq. (3), within the dipole approximation, yields for photoemission intensity with RH(+) or LH(−) polarized light

$$I_{\mathrm{RH/LH}} = \frac{a^2}{8c^2}\sum_i B_{ii} |\langle f|(\hat{\mathbf{x}}' \pm i\hat{\mathbf{y}}')\cdot\mathbf{p}|i\rangle|^2. \tag{6}$$

The dichroism signal D_S, that is, the difference between intensity for left- and right-handed polarizations, is

$$D_S = \frac{a^2}{8c^2}\sum_i B_{ii}[|\langle f|(\hat{\mathbf{x}}' + i\hat{\mathbf{y}}')\cdot\mathbf{p}|i\rangle|^2 - |\langle f|(\hat{\mathbf{x}}' - i\hat{\mathbf{y}}')\cdot\mathbf{p}|i\rangle|^2]$$

$$= -\frac{a^2}{2c^2}\sum_i B_{ii}\Im\{\langle i|\hat{\mathbf{x}}'\cdot\mathbf{p}|f\rangle\langle f|\hat{\mathbf{y}}'\cdot\mathbf{p}|i\rangle\}. \tag{7}$$

It is a straightforward task to derive the selection rules for D_S arising from the crystal symmetry. If the wave vectors of the incident photon and the photoelectron lie on a mirror plane or a glide plane, either $\langle i|\hat{\mathbf{x}}'\cdot\mathbf{p}|f\rangle$ or $\langle i|\hat{\mathbf{y}}'\cdot\mathbf{p}|f\rangle$ is zero,[20,21] and thus the D_S is zero. This is valid beyond the dipole approximation. It is important to interpret the final state correctly. In the simplest approximation, where the final state is treated as a plane wave, the expression $\langle i|\hat{\mathbf{x}}'\cdot\mathbf{p}|f\rangle\langle f|\hat{\mathbf{y}}'\cdot\mathbf{p}|i\rangle$ is real and the D_S is zero.

Defining θ as the angle between photon wave vector $\mathbf{q}$ and surface normal $\mathbf{n}$, and ϕ as the angle between $\mathbf{q}_\parallel$ and x axis, transformation from the coordinate system attached to the photon to the right handed coordinate system of the sample in Fig. 1(a), where $\hat{\mathbf{z}} \| \mathbf{n}$, involves

$$\hat{\mathbf{x}}' = \cos(\phi)\cos(\theta)\hat{\mathbf{x}} + \sin(\phi)\cos(\theta)\hat{\mathbf{y}} + \sin(\theta)\hat{\mathbf{z}},$$

$$\hat{\mathbf{y}}' = -\sin(\phi)\hat{\mathbf{x}} + \cos(\phi)\hat{\mathbf{y}},$$

$$\hat{\mathbf{z}}' = \cos(\phi)\sin(\theta)\hat{\mathbf{x}} + \sin(\phi)\sin(\theta)\hat{\mathbf{y}} - \cos(\theta)\hat{\mathbf{z}}. \tag{8}$$

Expression (7) for D_S in the sample's coordinate system is

$$D_S = -\frac{a^2}{2c^2}\sum_i B_{ii}\Im\{\cos\phi\sin\theta M_{fi}^{(z)}M_{if}^{(y)} - \sin\phi\sin\theta M_{fi}^{(z)}M_{if}^{(x)} + \cos\theta M_{fi}^{(x)}M_{if}^{(y)}\}, \tag{9}$$

where $M_{if}^{(j)} = \langle f|\hat{\mathbf{j}}\cdot\mathbf{p}|i\rangle$. Thus, for arbitrarily chosen experimental setup, D_S becomes a rather complicated function.

Theory of ARPES calculation with circularly polarized light is in details published by Ishii and Yamada,[15] though their derivation applies only to normal incidence setup. Following Hopkinson *et al.*,[22] the perturbation operator [Eq. (4)] for a circularly symmetric muffin-tin potential is given in spherical harmonic representation,

$$\Delta = \frac{a}{\omega c}\frac{dV}{dr}\frac{2\pi}{3}\sum_{m''=-1}^{1} Y_{1m''}^*(\hat{\mathbf{e}})Y_{1m''}(\mathbf{r}-\mathbf{c}_j)e^{i\mathbf{q}\cdot\mathbf{c}_j}, \tag{10}$$

where $\mathbf{c}_j$ is the position of atom j in the unit cell. A local dipole approximation is made by replacing slowly varying $e^{i\mathbf{q}\cdot r}$ with its value at the center of the atom. Initial and final states are written in spherical harmonic representation,

$$|i\rangle = \sum_{lm} A_{1lm}R_l(|\mathbf{r}-\mathbf{c}_j|)Y_{lm}(\mathbf{r}-\mathbf{c}_j),$$

$$|f\rangle = \sum_{l'm'} A_{2l'm'}R'_l(|\mathbf{r}-\mathbf{c}_j|)Y_{l'm'}(\mathbf{r}-\mathbf{c}_j). \tag{11}$$

When the matrix element $\langle f|\Delta|i\rangle$ is calculated, angular integration between spherical harmonics yields

$$D_{lml'm'} = \frac{2\pi A}{3c}Y_{1m'-m}^*(\hat{\mathbf{e}})\int d\Omega Y_{l'm'}^* Y_{1,m'-m}Y_{lm}. \tag{12}$$

Polarization of the incident photon in $Y_{1m'-m}^*(\hat{\mathbf{e}})$, which, except for the small surface barrier contribution,[18] is the only part of the program where polarization is involved, determines atomic selection rules for quantum number m. $\Delta m=-1$ for LH light and $\Delta m=+1$ for RH light. These rules are defined in the coordinate system of the photon. Transformation to the coordinate system attached to the sample is given in Eq. (8).

Thus, both the atomic selection rules and the selection rules due to crystal symmetry play a role. The symmetry selection rules determine zeros of the D_S. The atomic selection rules can be applied for states with strong atomic character, but only with a special experimental geometry. The simplest is the normal incidence setup where $\hat{\mathbf{e}}=\frac{1}{\sqrt{2}}(\hat{\mathbf{x}}\pm i\hat{\mathbf{y}})$.

The relevant technical details of our computations are as follows. Crystal structure of Bi2212 is assumed to be perfectly tetragonal. Surface structure is assumed to terminate in the Bi-O layer. The crystal potential was first obtained self-consistently within the Korringa-Kohn-Rostoker scheme.[23,24] This self-consistent local-density-approximation (LDA)-based potential is slightly modified in that the Bi-O pockets around the $(\pi,0)$ point are lifted above the Fermi energy to account for their absence in the experimental spectra.[25]

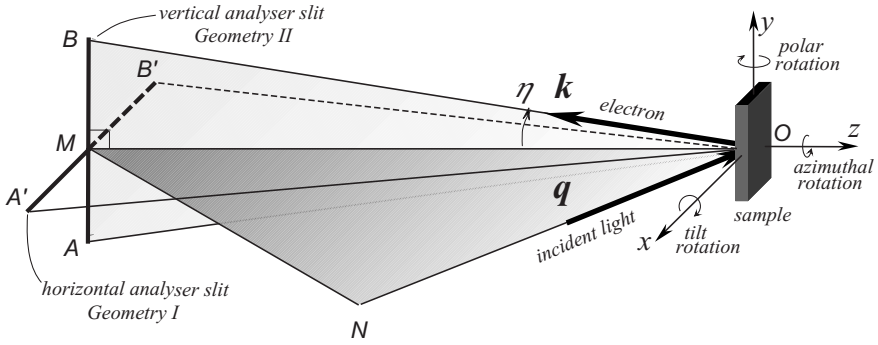

FIG. 2. Experimental geometry. The sample is mounted on the head of the cryomanipulator, which is represented by the black cuboid, and can be rotated around all three axes to project necessary part of momentum space onto the analyzer entrance slit AB ($A'B'$). The angle MON between the incident light **q** and the forward direction of the analyzer is fixed to 45°. In geometry I, the analyzer slit $A'B'$ is horizontal, while in Geometry II, the slit is set vertical along the AB direction.

These modifications are not expected to change the scattering properties of the final state electron.[14]

III. EXPERIMENT

Two types of experimental setups were used. The measurements with normal incidence, which we call here geometry I, were performed at the 4.2R beam line of the ELETTRA storage ring using circularly polarized light from the elliptical wiggler undulator and Scienta SES-100 electron-energy analyzer. The overall average resolution in momentum-energy space was set to 0.01 $Å^{-1} \times 0.02$ $Å^{-1} \times 40$ meV. Measurements in geometry II were done at the SIS 9L beam line at the Swiss Light Source using the same electron analyzer. The only difference between the two geometries was that in geometry I, the analyzer entrance slit was set horizontal, while in geometry II, the analyzer slit was vertical. For details, see Fig. 2. The overall average resolution for geometry II was 0.02 $Å^{-1} \times 0.02$ $Å^{-1} \times 20$ meV. High quality overdoped samples $(BiPb)_2Sr_2CaCu_2O_{8+\delta}$ with T_c=72 K and $Bi_2Sr_2CaCu_2O_{8+\delta}$ with T_c=69 K were mounted on the three-axes cryomanipulator and cleaved *in situ*. Mapping procedure was realized via gradual change of the manipulator azimuthal or polar angle, depending on the geometry. All the data presented here were collected below T_c at $T \approx 30$ K within 12 h after cleavage.

IV. RESULTS

In Fig. 3, theoretical and experimental Fermi surface (FS) maps are compared within normal incidence setup. Excitation energy was 20 eV. Figure 3(a) and 3(b) show theoretical and experimental FS maps with left-handed polarization and Figs. 3(c) and 3(d) with right-handed circular polarization. Figure 3(e) and 3(f) show the dichroism signal. The part of the $k_{\|}$ space which was studied experimentally is marked with a contour line in the calculated FS maps. In this part of FS, the computations predict that the relative photoelectron intensity is quite low, with higher intensities at antinodal point $(\pi/a, 0)$ in the first Brillouin zone. The level of agreement between calculated and measured intensities is good. Left-handed polarization enhances the intensity at nodal point B and right handed at nodal point A. In the D_S map around nodal point A, the bands are bright, indicating positive D_S, while around point B bands are dark, indicating

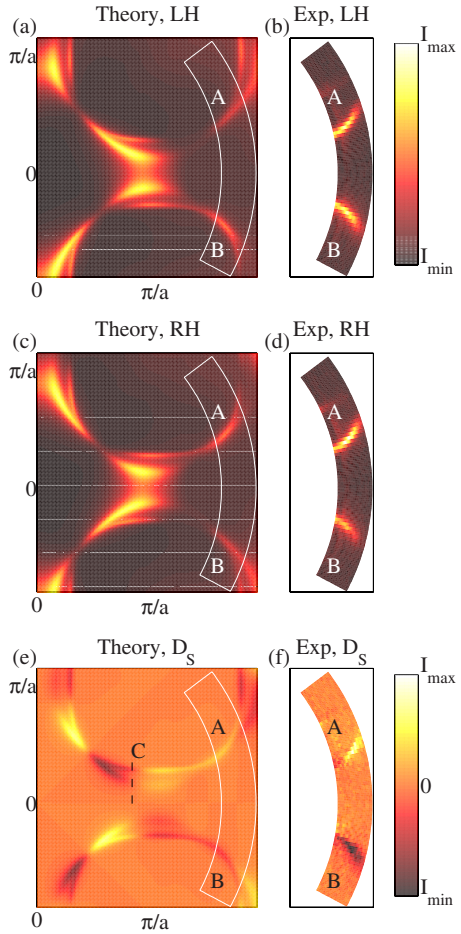

FIG. 3. (Color online) Comparison between experimental and theoretical FS maps, normal incidence setup, $h\nu$=20 eV, sample $(BiPb)_2Sr_2CaCu_2O_{8+\delta}$ with T_c=72 K. (a) Calculated with left-handed circular polarization. (b) Experiment, left-handed polarization. (c) Calculated, right-handed polarization. (d) Experiment, right-handed polarization. (e) Calculated, dichroism signal. (f) Experiment, dichroism signal.

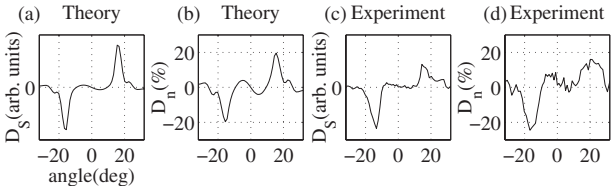

FIG. 4. Dichroism signals D_S and normalized D_n integrated through the experimentally probed part of $\mathbf{k}_\parallel$ space in Fig. 3 and plotted as a function of electron's escape angle. (a) Calculated D_S. (b) Calculated D_n. (c) Experimental D_S. (d) Experimental D_n.

negative D_S. The FS maps with different helicities are mirror images, and the dichroism maps are antisymmetric with respect to mirror plane at $k_y=0$. This is a property of circularly polarized light, whose direction is inverted in a reflection. In Fig. 3, reflection operator corresponding to the mirror plane is $y \rightarrow -y$. Operation to the polarization vector yields $\hat{\mathbf{x}} \pm i\hat{\mathbf{y}} \rightarrow \hat{\mathbf{x}} \mp i\hat{\mathbf{y}}$. Thus, the direction of circular polarization is inversed and dichroism signals measured with different helicities must be mirror images.

There are also differences between theoretical and experimental D_S maps. In calculated D_S map, the antibonding band changes its sign at the right side edge of the experimentally probed area, where the bonding band still has the same sign. In the experiment, the sign of D_S seems to change at the left side edge of the measured area. These types of differences are to be expected. The dichroism signal is a difference between two measurements, which makes it very sensitive to experimental setup and, which is to be discussed more specifically later, computational parameters. This sensitivity is even enhanced in the probed part of $\mathbf{k}_\parallel$ space, where computations predict that intensities are generally small.

Figure 4 shows integrated D_S as a function of in-plane escape angle. Integration is carried out through the measured area outlined in Fig. 3(e). Both the unnormalized $D_S=I_r-I_l$ and normalized $D_n=(I_r-I_l)/(I_r+I_l)$ are plotted. Calculated results are in Figs. 4(a) and 4(b) and experimental spectra in Figs. 4(c) and 4(d). For unnormalized D_S, the units are arbitrary. To simulate the experimental background noise, a constant background signal has been added to theoretical spectra. This allows direct comparison of normalized dichroism signal D_n. These plots show even more clearly that dichroism signal is antisymmetric with respect to reflection in $k_y=0$ plane. The maximum value of both experimental and calculated D_n is $\sim$20%. We also calculated D_n in the first Brillouin zone where intensities and also the D_S are stronger. There the maximum value of D_n was larger than 50%.

As was pointed out, the D_S is sensitive to experimental setup and computational parameters. We studied the changes of the dichroism signal as a function of final state width Σ_f''. In the part of $k_\parallel$ space, where intensities are high, the variations of D_S as a function of Σ_f'' are small, but in the experimentally studied area there are variations especially at higher values of $\Sigma_f'' > 3$ eV. High values broaden features in the dichroism map and decrease the value of normalized D_n. This can be explained with the increased width of the final state, but larger Σ_f'' also decreases the penetration depth of the final state electrons and makes the final state more plane-wave-like, which decreases D_S. As was shown in Sec. II, D_S

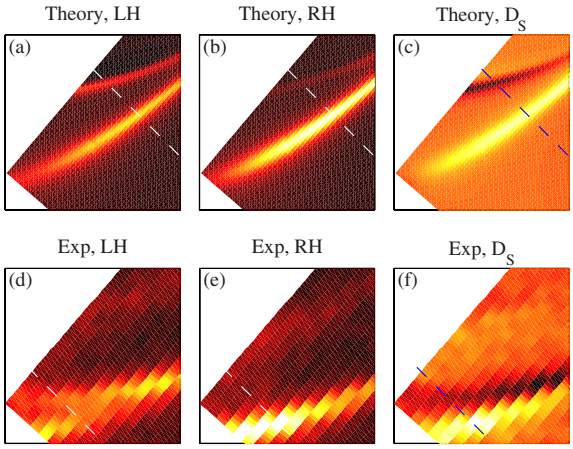

FIG. 5. (Color online) Comparison between experimental and theoretical FS maps, geometry II, $h\nu=50$ eV, sample $Bi_2Sr_2CaCu_2O_{8+\delta}$ with $T_c=69$ K. (a) Calculated, LH light. (b) Calculated, RH light. (c) Calculated map of the dichroism signal. (d) Experiment, LH light. (e) Experiment, RH light. (f) Experimental map of the dichroism signal.

is zero if the final state is a plane wave. Comparison between computational and experimental D_S patterns and normalized D_n could be a way to check the value of Σ_f''. Σ'' used for the shown figures were 100 meV for the initial state and 2.0 eV for the final state.

In Fig. 5, comparison is made within geometry II that was described in Sec. III. FS maps were measured and calculated in the area between the antinodal $(-\pi/a, 0)$ and nodal $(-\pi/2a, \pi/2a)$ points. Theoretical FS maps with LH light, RH light, and their difference D_S are in Figs. 5(a)–5(c). Corresponding experimental maps are in Figs. 5(d)–5(f). The modified LDA FS is different from the experimental one, and especially the bilayer splitting is overestimated, but focusing to the intensities instead of the FS shape reveals that the calculated intensity patterns are in good correspondence with the experiments. RH light enhances the antibonding band, while the bonding band is clearly visible only with LH light. Thus, contrary to Fig. 3, the bonding and antibonding bands have a different sign of D_S in Figs. 5(c) and 5(f).

In Fig. 6, the momentum distribution curves (MDCs) along the dashed lines in Fig. 5 are shown. Because of the different shapes of theoretical and experimental Fermi surfaces, the cuts are not made exactly at the same $\mathbf{k}_\parallel$ position, but along lines that are structurally equivalent. Again, to be able to compare D_n, a constant background signal has been added to theoretical spectra. The two bilayer split bands are clearly seen in Fig. 6(a) that is calculated with LH light. The lower peak on the left is from the bonding band, and the higher one on the right is from the antibonding band. In Fig. 6(b), calculated with RH light, the peak from the antibonding band is higher, and the peak from the bonding band is very low. The same behavior can be seen experimentally in Figs. 6(e) and 6(f), but because of the smaller bilayer splitting in experiments, it is difficult to distinguish the peaks corresponding to different bands. In the D_S, both calculated in Fig. 6(c) and experimental in Fig. 6(g), the split bands have different signs and are clearly distinquishable. In the experi-

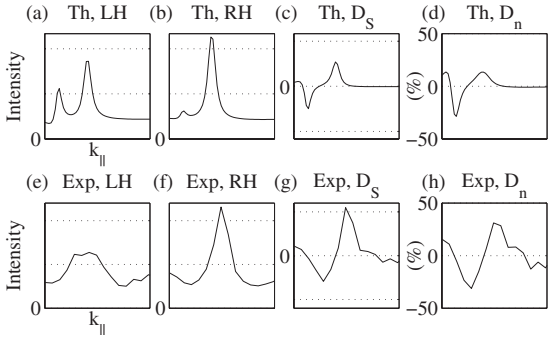

FIG. 6. MDCs along dashed lines in Fig. 5, $h\nu$=50 eV. (a) Calculated, LH light. (b) Calculated, RH light. (c) Calculated D_S. (d) Calculated D_n. (e) Experiment, LH light. (f) Experiment, RH light. (g) Experimental D_S. (h) Experimental D_n.

ment, D_S is even stronger than in calculations. D_n is in Figs. 6(d) and 6(h). In the calculated D_n, the first peak in the positive side is a numerical artifact (both LH and RH intensities are low). The height of the peak from the bonding band is approximately 30%. The peak from the antibonding band is lower but wider. Experimentally, both peaks have the same height of ~30%. Neither the calculated D_S nor D_n are sensitive to changes in the imaginary parts of the self-energies Σ_i and Σ_f. The values used for the shown spectra were 25 meV for initial states and 1.5 eV for final states.

We have investigated excitation energy dependence of the dichroism signal in Fig. 7. Photoelectron intensity was calculated along the dashed line, labeled with C, in Fig. 3(e) at k_x=0.661/Å, and recalculated with different values of excitation energy. Photon flux, angles of incidence, and computational parameters were held constant. Polar angle of the photon vector $\mathbf{q}$ was 30°, with $\mathbf{q}_\parallel$ parallel to k_x. Σ_i'' was 50 meV and Σ_f'' was 2 eV. The results are plotted in a colormap as a function of k_y and $h\nu$. Figure 7(a) shows the photoelectron intensity calculated with left-handed polarization and Fig. 7(b) with right-handed circular polarization. There

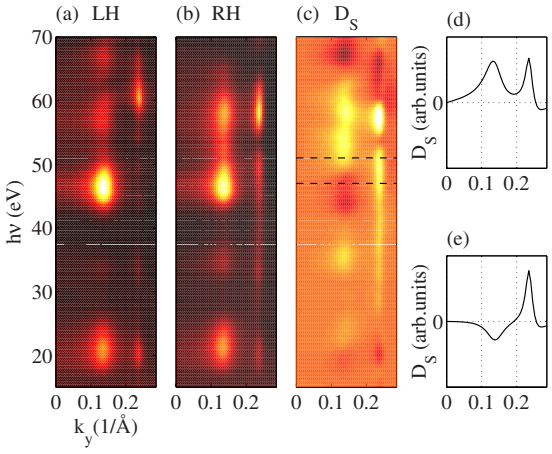

FIG. 7. (Color online) Photoelectron intensity calculated as a function of excitation energy at k_x=0.661/Å along the dashed line labeled with C in Fig. 3(e). (a) LH light. (b) RH light. (c) Map of D_S. (d) MDC of D_S at $h\nu$=51 eV, along the upper dashed line in (c). (e) MDC of D_S at $h\nu$=47 eV, along the lower dashed line in (c).

are no large differences with intensity patterns calculated with RH or LH light. Both photoelectron intensity maps show high intensity at resonance energies of ~30, ~46, and ~60 eV. Map of dichroism signal is in Fig. 7(c). D_S varies strongly as a function of photon energy, and the variations are considerably different for the bilayer split bands. This can be expected because the intensity difference of the bilayer split bands in Figs. 7(a) and 7(b) varies largely as a function of photon energy, which has also been shown to occur with linearly polarized light.[26,27]

Figures 7(d) and 7(e) show MDCs of D_S at excitation energies 51 eV and 47 eV. These positions have also been plotted with dashed lines in Fig. 7(c). The units are arbitrary, but the intensity axis are the same in both figures. In Fig. 7(d), the bilayer split bands have the same sign of D_S, whereas in Fig. 7(e), the sign is the opposite. These results verify that, as a result of matrix element effects, within certain experimental setup and photon energies the D_S for the bilayer split bands may have the opposite sign. This can be used to study the properties of the split bands. As was mentioned in the Introduction, it was used to study bilayer splitting at nodal direction, where the bands are only very weakly split and very difficult to distinguish by common ARPES techniques with linearly polarized light.[6]

The difference between D_S from antibonding and bonding bands arises naturally as an interference effect. To qualitatively describe the origin of the different D_S for the bilayer split bands, let us consider the initial state as a simple Bloch state. The relevant initial states are predominantly Cu $3d_{x^2-y^2}$ hybridized with oxygen $2p_{x,y}$. For our purposes, the initial state is a linear combination of two relevant hybrid states $\phi_1(\mathbf{r})$ and $\phi_2(\mathbf{r})$ at layers 1 and 2 parallel to the surface,

$$\psi_{b/ab}(\mathbf{k}_\parallel,\mathbf{r}) = \sum_{\boldsymbol{\tau}_\nu} e^{i\mathbf{k}_\parallel\cdot\boldsymbol{\tau}_\nu}[\phi_1(\mathbf{r}-\boldsymbol{\tau}_\nu) \pm \phi_2(\mathbf{r}-\boldsymbol{\tau}_\nu)], \quad (13)$$

where $\mathbf{k}_\parallel$ is a wave vector parallel to the surface and $\boldsymbol{\tau}_\nu$ is the position of the νth two-dimensional primitive cell. "+" sign refers to bonding state $\psi_b(\mathbf{k}_\parallel,\mathbf{r})$ and "−" to antibonding state $\psi_{ab}(\mathbf{k}_\parallel,\mathbf{r})$. A transition matrix with circularly polarized light from these states to a time-reversed LEED state $\psi_f(\mathbf{k}_\parallel,\mathbf{r})$, if off-site matrix elements are neglected, is

$$\langle f|(\hat{\mathbf{x}}' \pm i\hat{\mathbf{y}}')\cdot\mathbf{p}|b\rangle \propto M_{1,f}^{(x)} \pm iM_{1,f}^{(y)} + M_{2,f}^{(x)} \pm iM_{2,f}^{(y)},$$

$$\langle f|(\hat{\mathbf{x}}' \pm i\hat{\mathbf{y}}')\cdot\mathbf{p}|ab\rangle \propto M_{1,f}^{(x)} \pm iM_{1,f}^{(y)} - M_{2,f}^{(x)} \mp iM_{2,f}^{(y)}, \quad (14)$$

where matrix elements between the two hybrid states and final state are denoted as $M_{1,f}^{(x)}=\langle f|\hat{\mathbf{x}}'\cdot\mathbf{p}|1\rangle=\langle f|p_x|1\rangle$, $M_{1,f}^{(y)}=\langle f|p_y|1\rangle$, and $M_{2,f}^{(x)}$, $M_{2,f}^{(y)}$, respectively. Here, it is assumed that when the antibonding and bonding states are not largely separated, the final state for both states is similar. The difference between the transition matrix elements is that for the antibonding band, the latter molecular matrix elements change their sign. D_S for these states can be straightforwardly derived.

$$D_S^b \propto -\Im[M_{1,f}^{(x)*}M_{1,f}^{(y)}] - \Im[M_{1,f}^{(x)*}M_{2,f}^{(y)}] - \Im[M_{2,f}^{(x)*}M_{1,f}^{(y)}] - \Im[M_{2,f}^{(x)*}M_{2,f}^{(y)}],$$

$$D_S^{ab} \propto -\Im[M_{1,f}^{(x)*}M_{1,f}^{(y)}] + \Im[M_{1,f}^{(x)*}M_{2,f}^{(y)}] + \Im[M_{2,f}^{(x)*}M_{1,f}^{(y)}] - \Im[M_{2,f}^{(x)*}M_{2,f}^{(y)}]. \quad (15)$$

The interference terms in these equations have different signs. This little model explains how D_S for antibonding and bonding states can, even in the simplest case, be very different.

V. CONCLUSIONS

We consider the emission of ARPES spectra from Bi2212 with circularly polarized light. A direct comparison between theoretical and experimental data at two excitation energies shows that circular dichroism in the angular distribution is largely reproduced by one-step simulations in the dipole approximation. Calculations predict a large variation of the dichroism signal as a function of excitation energy, and distinct responses from the two bilayer split bands. The large magnitude of the normalized dichroism signal, which was found to be higher than 50% in the normal incidence setup, suggests that circular dichroism within the dipole transition is large, and ARPES matrix element effects should not be ignored in the studies addressing the exotic properties of the ground state.

ACKNOWLEDGMENTS

This work benefited from the Institute of Advanced Computing (IAC), Tampere and Techila Technologies computational solutions. We also want to thank C. Grazioli, S. Turchini, and L. Patthey for their support during experimental measurements at ELETRA and SLS synchrotron facilities, and J. Nieminen for valuable comments on the paper. One of us (V.A.) acknowledges Väisälä Foundation, Pirkanmaa Trust, Tekniikan Edistämissäätiö, and Magnus Ehrnrooth Foundation for financial support.

[1] C. M. Varma, Phys. Rev. B **61**, R3804 (2000).
[2] M. E. Simon and C. M. Varma, Phys. Rev. Lett. **89**, 247003 (2002).
[3] S. V. Borisenko, A. A. Kordyuk, A. Koitzsch, M. Knupfer, J. Fink, H. Berger, and C. T. Lin, Nature (London) **431** (2004).
[4] S. V. Borisenko, A. A. Kordyuk, A. Koitzsch, T. K. Kim, K. A. Nenkov, M. Knupfer, J. Fink, C. Grazioli, S. Turchini, and H. Berger, Phys. Rev. Lett. **92**, 207001 (2004).
[5] N. P. Armitage and J. Hu, Philos. Mag. Lett. **84**, 105 (2004).
[6] S. V. Borisenko, A. A. Kordyuk, S. Legner, T. K. Kim, M. Knupfer, C. M. Schneider, J. Fink, M. S. Golden, M. Sing, R. Claessen *et al.*, Phys. Rev. B **69**, 224509 (2004).
[7] S. V. Borisenko, A. A. Kordyuk, A. Koitzsch, J. Fink, J. Geck, V. Zalobotnyy, M. Knupfer, B. Büchner, H. Berger, M. Falub *et al.*, Phys. Rev. Lett. **96**, 067001 (2006).
[8] B. Ritchie, Phys. Rev. A **12**, 567 (1975).
[9] N. A. Cherepkov, Chem. Phys. Lett. **87**, 344 (1982).
[10] G. Schönhense, Phys. Scr., T **T31**, 255 (1990).
[11] N. Chandra, Phys. Rev. A **39**, 2256 (1989).
[12] N. A. Cherepkov, Z. Phys. D: At., Mol. Clusters **7**, 271 (1987).
[13] A. Bansil and M. Lindroos, Phys. Rev. Lett. **83**, 5154 (1999).
[14] M. Lindroos, S. Sahrakorpi, and A. Bansil, Phys. Rev. B **65**, 054514 (2002).
[15] A. Ishii and K. Yamada, Surf. Sci. **363**, 262 (1996).
[16] M. Mulazzi, M. Hochstrasser, M. Corso, I. Vobornik, J. Fujii, J. Osterwalder, J. Henk, and G. Rossi, Phys. Rev. B **74**, 035118 (2006).
[17] C. Caroli, D. Lederer-Rozenblatt, B. Roulet, and D. Saint-James, Phys. Rev. B **8**, 4552 (1973).
[18] J. B. Pendry, Surf. Sci. **57**, 679 (1976).
[19] M. A. V. Hove, W. H. Weinberg, and C. M. Chan, *Low-Energy Electron Diffraction* (Springer, Berlin, 1986).
[20] V. Arpiainen and M. Lindroos, Phys. Rev. Lett. **97**, 037601 (2006).
[21] J. Hermanson, Solid State Commun. **22**, 9 (1977).
[22] J. F. L. Hopkinson, J. B. Pendry, and D. J. Titterington, Comput. Phys. Commun. **19**, 69 (1980).
[23] S. Kaprzyk and A. Bansil, Phys. Rev. B **42**, 7358 (1990).
[24] A. Bansil, S. Kaprzyk, P. E. Mijnarends, and J. Tobola, Phys. Rev. B **60**, 13396 (1999).
[25] V. Bellini, F. Manghi, T. Thonhauser, and C. Ambrosch-Draxl, Phys. Rev. B **69**, 184508 (2004).
[26] M. C. Asensio, J. Avila, L. Roca, A. Tejeda, G. D. Gu, M. Lindroos, R. S. Markiewicz, and A. Bansil, Phys. Rev. B **67**, 014519 (2003).
[27] M. Lindroos, R. S. Markiewicz, and A. Bansil, Phys. Rev. B **69**, 140505(R) (2004).